Constituent contribution to the magnetocrystalline anisotropy in $Mn(Al_{1-x}Ga_x)$

Cite as: AIP Advances 13, 025309 (2023); doi: 10.1063/9.0000408
Submitted: 30 September 2022 • Accepted: 16 November 2022 •
Published Online: 3 February 2023

X. B. Liu,[a] D. H. Ryan,[b] and Z. Altounian

AFFILIATIONS

Centre for the Physics of Materials and Department of Physics, McGill University, Montreal, Quebec H3A 2T8, Canada

Note: This paper was presented at the 67th Annual Conference on Magnetism and Magnetic Materials.
[a]**Present address:** Centre for the Physics of Materials and Department of Physics, McGill University, Montreal, Quebec H3A 2T8, Canada. **Author to whom correspondence should be addressed:** liux@ameslab.gov
[b]dhryan@physics.mcgill.ca

ABSTRACT

The phase stability and magnetocrystalline anisotropy (MCA) of tetragonal $Mn(Al_{1-x}Ga_x)$ with the $L1_0$-type structure (P4/mmm) has been studied using first-principles density functional calculations. The calculated decomposition energy indicates that partial replacement of Al by Ga suppresses the formation of $Mn_5(Al,Ga)_8$ and enhances the thermal stability of the $L1_0$ phase while the total magnetic moment per formula unit (f.u.) remains almost unchanged. The site- and atomic-resolved MCA calculations show that the MCA energy (MAE) comes mainly from the Mn atoms, and the total MAE increases from 0.25 meV/f.u. (x = 0) to 0.34 meV/f.u (x = 1). Spin resolved MCA and band structure calculations indicate that the high MCA is mainly due to spin flipping behavior near Fermi level. The derived effective magnetic anisotropy field increases from 37 kOe (x = 0) to 46 kOe (x = 1), in agreement with experiments. Doping with Ga improves the thermal stability of the $L1_0$ structure and enhances the magnetic anisotropy field, which facilitates developing high coercivity Mn-Al magnets.

I. INTRODUCTION

MnAl has gained attention as a potential rare-earth-free hard magnet.[1–4] Tetragonal MnAl with the $L1_0$-type structure (P4/mmm No. 123) displays good intrinsic hard magnetic properties such as large magnetization (M_S = 110 emu/g), high magnetocrystalline anisotropy field (H_A = 40 kOe), and moderate Curie temperature (T_C = 600 K).[5,6] In the perfectly ordered $L1_0$ structure, Al and Mn occupy the 1*a* (0, 0, 0) and 1*d* (0.5, 0.5, 0.5), sites respectively. Tetragonal MnAl is a metastable phase, with a narrow composition window of $Mn_{1+x}Al$ (x = 0.05–0.4).[7,8] The excess Mn atoms partially substitute for Al on the 1*a* site, and couple antiferromagnetically with the Mn atoms at the 1*d* site, as seen by neutron diffraction.[9] Similar situations are observed in the isostructural $Mn_{1+x}Ga$ compounds.[9,10]

The tetragonal MnAl phase can be prepared by conventional arc-melting followed by high temperature annealing (e.g. at 1323 K), or by melt-spinning with a subsequent low temperature heat treatment (e.g. at 723 K).[1,3] However, the as-prepared magnet is isotropic and has low coercivity (less than 0.5 kOe). Thermal-mechanical processing such as swaging and hot extrusion is needed to introduce c-axis crystal texture. The highest maximum energy product is 7–8 MGOe for warm-extruded Mn-Al-C magnet.[11] The challenge is that the metastable $L1_0$-phase easily decomposes into pure manganese (β-Mn) and a Cr_5Al_8-type ($R3m$) Mn-Al phase during high temperature processing.[12] Stabilizing the $L1_0$ structure is necessary to develop a high performance MnAl bulk magnet using thermo-mechanical processing.

The $L1_0$ structure can be stabilized via doping with carbon or partial replacement of Al by Ga.[2,6,9,13,14] However, doping with carbon reduces both the Curie temperature and the magnetocrystalline anisotropy (MCA).[6] $L1_0$-type $Mn_{1+x}Ga$ displays good hard magnetic properties, but the nearly 50% of critical element Ga discourages industrial applications. Partial replacement of Al by Ga can increase the phase stability and improve the decomposition temperature and some limited but inconsistent experimental data on magnetic properties have been reported.[2,3] It is likely that the inconsistencies are related to different sample preparation and processing details. Ga-substituted $L1_0$-phases $Mn_{54.5}Al_{45.5-x}Ga_x$ (x = 0.0, 15.0, 25.0, 35.0, 45.5) have been prepared by melt spinning plus subsequent annealing.[3] Neutron diffraction results show that the most of Ga atoms occupy the Al site (1*a*), while a few of the Ga(Al) enter the Mn site (1*d*).[3,9] Moze *et al.* reported that the

magnetization decreases from 100 emu/g ($x = 0$) to 55 emu/g ($x = 12$) while the magnetic anisotropy field increases from about 47 kOe ($x = 0$) to 57 kOe ($x = 12$) in $Mn_{69.5}A1_{30.5-x}Ga_x$ (mass%) at room temperature.[9]

The metastable nature of the MnAl $L1_0$-phase promotes formation of structural defects and phase decomposition that degrade the hard magnetic properties. The magnetic properties of MnAl and MnGa have been calculated from first principles by several groups,[15–20] but detailed theoretical research on $Mn(Al_{1-x}Ga_x)$ has not been reported. In this work, we have studied the effect of a partial replacement of Al by Ga on the phase stability and MCA in $Mn(Al_{1-x}Ga_x)$ using first-principles density functional calculations. In particular, we focus on the different components contributed to MCA.

II. COMPUTATIONAL METHOD AND DETAILS

The stability of $L1_0$-phase was evaluated by the formation energy of the $L1_0$-phase, i.e., the energy difference between the total energy of $Mn(Al_{1-x}Ga_x)$ and that of the pure metals Mn, Al and Ga, $E_f = E_{L10} - E_{Mn} - (1-x)E_{Al} - xE_{Ga}$. Since MnAl often decomposes into manganese and Mn_5Al_8 at high temperature, the decomposition energy, E_{decomp}, was also calculated. E_{decomp} is defined as the difference between total energy of the decomposition products of Mn and $Mn_5(Al, Ga)_8$ and that of MnAl phase: $E_{decomp} = E_{L10} - \frac{3}{8}E_{Mn} - \frac{1}{8}E_{Mn_5(Al_{1-x}Ga_x)_8}$.

The magnetocrystalline anisotropy is a result of interaction between spin-orbit coupling (SOC) and crystal field.[21,22] There are several electronic structure methods to calculate the MCA within a density-functional theory framework.[19,20,23–27] One is a full self-consistent scheme which is based on the direct calculation of the total energy (including SOC) difference for the spin magnetic moments along two different crystallographic axis. For the tetragonal structure, the selected crystallographic axis is [001] and [110]. $E_{mca} = E_{110} - E_{001}$. A positive value means easy-axis magnetic anisotropy while a negative value indicates easy-plane MCA. Another approach is the so-called force theorem (FT) where the MCA is taken as the band energy difference obtained after a one-step diagonalization of the full Hamiltonian including SOC, starting from the well converged self-consistent scalar relativistic (without SOC) charge density. The FT approach can substantially reduces the computational cost. In 3*d* metallic alloys, the SOC band shifts are usually well described by second-order perturbation theory (SPT).[26–29] The MCA energy equals approximately to one half of the difference between spin-orbital energy E_{SOC} with spin quantization axis parallel to [110] and [001] crystal orientations, i.e. $E_{mca} = (E_{soc}^{110} - E_{soc}^{001})/2$.[29] The MCA calculation using SPT shows efficiency and accuracy comparable to the popular FT method. It works well for the system with weak spin-orbit interaction, e.g., 3*d* or 4*d* alloys.[19,20] Here we adopt the SPT approach to calculate MCA.

We perform the First-principles DFT calculations using the linear-muffin-tin orbitals (LMTO) method with a coherent potential approximation (CPA) to treat alloying behavior.[30–32] The exchange-correlation has been treated using the generalized gradient approximation (GGA) of Perdew-Burke-Ernzerhof.[33] The k-space integrations have been performed with the tetrahedron method.[34,35] A uniform mesh of 24 × 24 × 18 in the full Brillouin zone provided sufficient accuracy for the *k* integration.

The initial lattice constants for DFT calculation are derived by linearly fitting the experimental data of $Mn_{54.5}Al_{45.5-x}Ga_x$.[3] The fitted lattice constant *a* decreases slightly from 2.768 Å to 2.735 Å while *c* increases from 3.576 Å to 3.717 Å with *x* from 0 to 1. The lattice distortion is anisotropic, i.e., the ratio of lattice constants *a*/*c* decreases with Ga content. The unit cell was optimized with fixed crystal symmetry for the $L1_0$-phase.

III. RESULTS AND DISCUSSION

Figure 1(a) displays the Ga content dependence of the formation energy for $L1_0$ phase, E_f, in $Mn(Al_{1-x}Ga_x)$ alloys. E_f increases from about −570 meV/f.u. to −350 meV/f.u. with Ga content from $x = 0$ to 1. The negative E_f indicates that while the $L1_0$ phase is stable over the whole composition range, it becomes progressivly less stable relative to the pure metals (Mn, Al and Ga) with increasing Ga content. On the other hand, the decomposition energy, E_{decomp}, is positive for all Ga contents and increases from 60 meV/f.u. ($x = 0$) to 270 meV/f.u. ($x = 1$) indicating that $Mn(Al_{1-x}Ga_x)$ becomes more stable against decomposition into Mn and $Mn_5(Al, Ga)_8$ as gallium is added. For example, the decomposition energy, $E_{decomp.}$, increases from about 60 meV/f.u. for $x = 0$ to about 90 meV/f.u. for $x = 0.2$. Based on the thermodynamic relationship $E_{decomp.} = k_BT$ (k_B is Boltzmann constant), the decomposition temperature $T_{decomp.}$ increase from 696 K to 1044 K with increasing *x* from 0 to 0.2. These results agree with the experimental

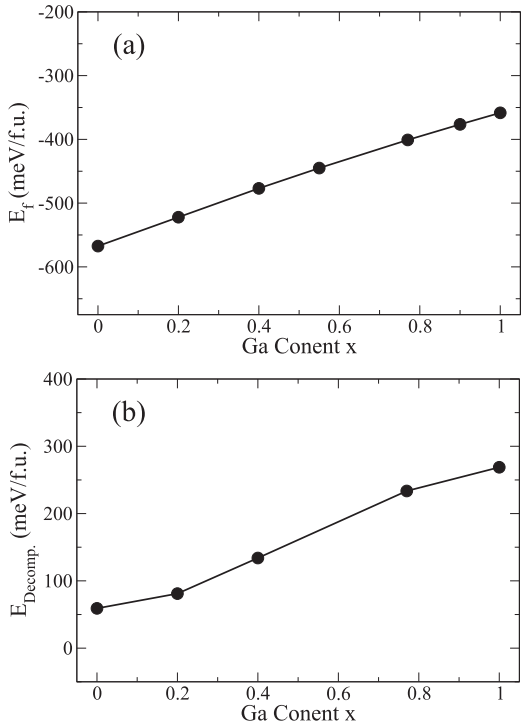

FIG. 1. Calculated formation energy (a) and decomposition energy (b) of $L1_0$ phase in $Mn(Al_{1-x}Ga_x)$ alloy.

fact that the MnAl decomposes while $Mn_{55}(Al_{1-x}Ga_x)_{45}$ with $x = 0.11–0.2$ is stable at 973 K.[2] As MnAl magnets are often annealed and/or extruded at a temperature from 773 K to 973 K.[3,11] A partial replacement of Al by 20% Ga is enough to stabilize the $L1_0$ phase during preparation processing. As discussed below, not only is this composition more stable, it also exhibits a larger MCA and a slightly higher magnetization (Figs. 2 and 3).

The calculated magnetic moment increases slightly from 2.37 μ_B ($x = 0$) to 2.5 μ_B ($x = 1$) per formula unit (f.u.) (Fig. 2). The total magnetic moment is almost completely contributed by Mn atoms and Al(Ga) has only a tiny induced moment. Experimentally, excess Mn is often added to stabilize the $L1_0$ structure during sample preparation. The excess Mn atoms occupy the Al(Ga) (1*a*) site with a much bigger moment of 3.2 μ_B and couple anitferromagnetically to the Mn at the 1*d* site.[9,10] We also calculated magnetic moment of $Mn_{1.2}(Al_{1-x}Ga_x)$ (Fig. 2). The magnetic moment is reduced by about 10% comparing with $Mn(Al_{1-x}Ga_x)$ alloys.

Figure 3 shows the calculated site-resolved MCA energy (MAE) as a function of Ga content. MAE is mainly contributed by the Mn atoms. With increasing Ga content, the MAE at both the Mn and the Al(Ga) sites increases and the total MAE increases from 0.25 meV/f.u. for $x = 0$ to 0.34 meV/f.u. for $x = 1$. The MAE at the Mn site increases rapidly with Ga content up to $x = 0.5$, then increases more slowly. However, the MAE at the Al(Ga) site increases almost linearly with Ga content.

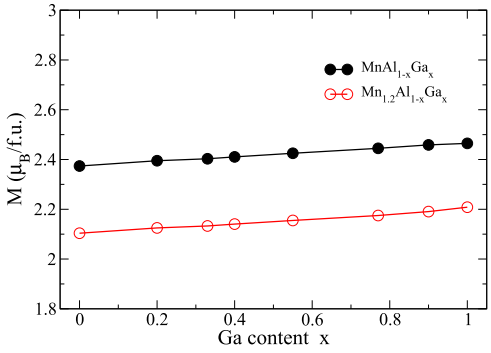

FIG. 2. Calculated magnetic moment in $Mn(Al_{1-x}Ga_x)$ and $Mn_{1.2}(Al_{1-x}Ga_x)$.

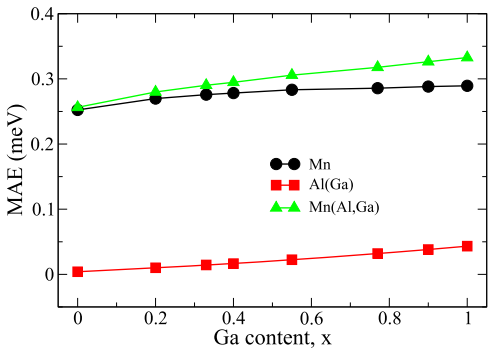

FIG. 3. Atomic site resolved MCA energy (MAE) in $Mn(Al_{1-x}Ga_x)$.

Within the second-order perturbation framework, the spin projected SOC energy includes the spin-conserving terms and the spin-flip ones. To gain more insight into the MCA in $Mn(Al_{1-x}Ga_x)$ alloys, E_{MAE} was resolved into spin components, i.e. spin-up ($E^{\uparrow\uparrow}_{MAE}$), spin-flipping ($E^{\uparrow\downarrow}_{MAE}$) and spin-down ($E^{\downarrow\downarrow}_{MAE}$) contributions (Fig. 4). All three components contribute positively to MAE. However, the main contribution to MAE comes from the spin flipping part. With increasing Ga contents from $x = 0$ to 1.0, the spin flipping contribution to the MAE increases rapidly from 0.12 meV/f.u. to 0.24 mev/f.u. while the spin-up (majority spin) electron contribution increases slightly from 0.033 meV/f.u. to about 0.048 meV/f.u. The contribution to MAE from spin-down electrons decreases from about 0.1 meV/f.u. to 0.024 mev/f.u. with increasing x. The MCA enhancement from spin-flipping transition is partially compensated by the reduced contribution from spin-down ones in $Mn(Al_{1-x}Ga_x)$ alloys. These competing contributions from different components of the MAE results in a moderate enhancement of MCA in $Mn(Al_{1-x}Ga_x)$ alloys.

Figure 5 displays the partial density of states (PDOS) for the Mn 3*d* electron states in $Mn(Al_{1-x}Ga_x)$ with $x = 0$ (black) and $x = 1$ (red). The spin up 3*d* Mn bands (majority spin) of MnGa ($x = 1$, red) are shifted to lower energies relative to the Fermi level of MnAl ($x = 0$,

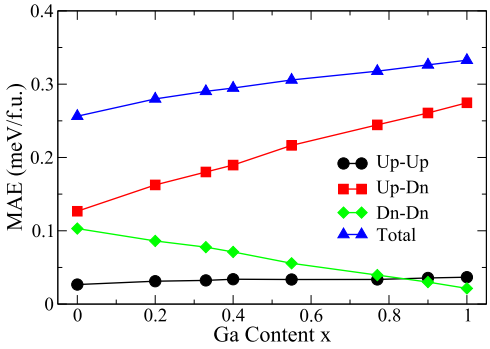

FIG. 4. Spin resolved MCA energy (MAE) in $Mn(Al_{1-x}Ga_x)$. The symbols of sphere, square, diamond and triangle stand for the MAE from spin-up ($E^{\uparrow\uparrow}_{MAE}$), spin-flip ($E^{\uparrow\downarrow}_{MAE}$), spin-down ($E^{\downarrow\downarrow}_{MAE}$), and total MAE, respectively.

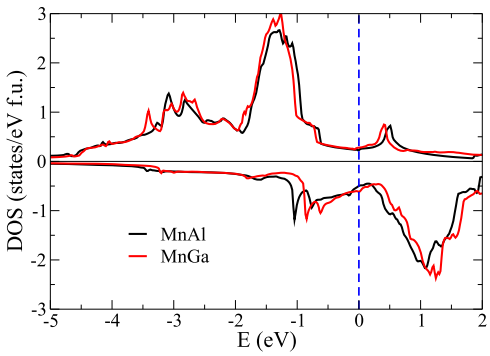

FIG. 5. Calculated partial density of states (PDOS) from Mn 3*d* electrons in $Mn(Al_{1-x}Ga_x)$ with $x = 0$ (black) and $x = 1$ (red). The dash vertical line shows the Fermi energy position.

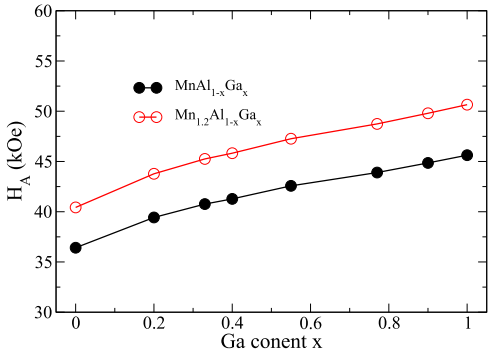

FIG. 6. Calculated magnetic anisotropy field, H_A, in $Mn(Al_{1-x}Ga_x)$ and $Mn_{1.2}(Al_{1-x}Ga_x)$.

black). On the other hand, the spin down (minority spin) bands move up in energy. The replacement of Al by Ga drives more 3*d* Mn electrons from the minority spin states into the majority spin bands. Although the total 3*d* electron number remains same, the spin splitting increases the net spin, resulting in a slight increment of magnetic moment in $Mn(Al_{1-x}Ga_x)$ with increasing Ga content.

The effective magnetic anisotropy field has been calculated using $H_A = 2K/\mu_0 M_s$. Here, H_A, K (E_{mca}), μ_0 and M_s are effective magnetic anisotropy field, MCA energy, magnetic susceptibility in vacuum and calculated magnetization, respectively. As shown in Fig. 6, H_A increases from 37 kOe (x = 0) to 46 kOe (x = 1), in $Mn(Al_{1-x}Ga_x)$. The magnetic anisotropy magnetic field, H_A, increases from about 41 to 51 kOe in $Mn_{1.2}(Al_{1-x}Ga_x)$, showing similar trends upon replacement of Al by Ga (Fig. 6). The calculated values of H_A are consistent with the experimental values.[9,18] The higher H_A for the samples with excess Mn is mainly related to their lower magnetic moment (Fig. 2).

IV. SUMMARY

In summary, first-principles studies indicate that the thermal stability of $L1_0$ structure can be enhanced though partial replacement of Al by Ga. The magnetocrystalline energy increases from 0.25 meV/f.u. for x = 0 to 0.34 meV/f.u. for x = 1.0 in $Mn(Al_{1-x}Ga_x)$ alloys. Spin resolved MCA and band structure calculations indicate that the microscopic origin of high MCA is mainly associated with the spin flipping behavior near Fermi level. Introducing excess Mn reduces the net magnetic moment and increases the magnetic anisotropy field. Doping with Ga improves the thermal stability of $L1_0$ phase and enhances the magnetic anisotropy field, which facilitates developing high coercivity Mn-Al magnets.

ACKNOWLEDGMENTS

Financial support for this work was provided by Fonds Québécois de la Recherche sur la Nature et les Technologies, and the Natural Sciences and Engineering Research Council (NSERC) Canada.

AUTHOR DECLARATIONS

Conflict of Interest

The authors have no conflicts to disclose.

Author Contributions

X.B. Liu: Conceptualization (equal); Investigation (equal); Writing – original draft (equal). **D.H. Ryan**: Conceptualization (equal); Funding acquisition (equal); Project administration (equal); Supervision (equal); Writing – review & editing (equal). **Z. Altounian**: Conceptualization (equal); Funding acquisition (equal); Methodology (equal); Project administration (equal); Supervision (equal).

DATA AVAILABILITY

The data that support the findings of this study are available from the corresponding author upon reasonable request.

REFERENCES

[1] A. Chaturvedi, R. Yaqub, and I. Baker, Journal of Physics Condensed Matter **26**, 064201 (2014).
[2] T. Mix, F. Bittner, K.-H. Müller, L. Schultz, and T. G. Woodcock, Acta Mater. **128**, 160 (2017).
[3] H. Zhao, W. Y. Yang, Z. Y. Shao, G. Tian, D. Zhou, X. P. Chen, Y. H. Xia, L. Xie, S. Q. Liu, H. L. Du, J. Z. Han, C. S. Wang, Y. C. Yang, and J. B. Yang, Journal of Alloys and Compounds **680**, 14 (2016).
[4] P. Zhao, L. Feng, K. Nielsch, and T. G. Woodcock, Journal of Alloys and Compounds **852**, 156998 (2021).
[5] A. J. J. Koch, P. Hokkeling, M. G. Steeg, and K. J. de Vos, J. Appl. Phys. **31**, S75 (1960).
[6] L. Pareti, F. Bolzoni, F. Leccabue, and A. E. Ermakov, J. Appl. Phys. **59**, 3824 (1986).
[7] H. Kōno, Journal of the Physical Society of Japan **13**, 1444 (1958).
[8] T. Massalski and U. Kattner, *Binary Alloy Phase Diagrams* (ASM International, 1990).
[9] O. Moze, L. Pareti, and A. E. Ermakov, J. Appl. Phys. **63**, 4616 (1988).
[10] D. H. Ryan, M. Yue, C. B. Boyer, X. B. Liu, Q. Lu, H. Zhang, C. Li, M. Wang, and Z. Altounian, Scientific Reports **7**, 646 (2017).
[11] T. Ohtani, N. Kato, S. Kojima, K. Kojima, Y. Sakamoto, I. Konno, M. Tsukahara, and T. Kubo, IEEE Transactions on Magnetics **13**, 1328 (1977).
[12] J. H. Huang and P. C. Kuo, Materials Science and Engineering: B **14**, 75 (1992).
[13] H. Fang, J. Cedervall, F. J. M. Casado, Z. Matej, J. Bednarcik, J. Ångström, P. Berastegui, and M. Sahlberg, J. Alloys Compd. **692**, 198 (2017).
[14] T. Mix and T. G. Woodcock, Results in Materials **5**, 100068 (2020).
[15] A. Sakuma, J. Magn. Magn. Mater. **187**, 105 (1998).
[16] J. H. Park, Y. K. Hong, S. Bae, J. J. Lee, J. Jalli, G. S. Abo, N. Neveu, S. G. Kim, C. J. Choi, and J. G. Lee, Journal of Applied Physics **107**, 09A731 (2010).
[17] A. Edstrom, J. Chico, A. Jakobsson, A. Bergman, and J. Rusz, Physical Review B - Condensed Matter and Materials Physics **90**, 014402 (2014).
[18] X. Liu, D. H. Ryan, M. Wang, Q. Lu, H. Zhang, M. Yue, and Z. Altounian, AIP Advances **7**, 056216 (2017).
[19] L. Ke, Physical Review B **99**, 054418 (2019).
[20] M. Blanco-Rey, J. I. Cerdá, and A. Arnau, New Journal of Physics **21**, 073054 (2019).
[21] K. Yosida, A. Okiji, and S. o. Chikazumi, Prog. Theor. Phys. **33**, 559 (1965).
[22] K. H. J. Buschow, Rep. Prog. Phys. **54**, 1123 (1991).
[23] G. H. O. Daalderop, P. J. Kelly, and M. F. H. Schuurmans, Physical Review B **41**, 11919 (1990).
[24] C. Li, A. J. Freeman, H. J. F. Jansen, and C. L. Fu, Physical Review B **42**, 5433 (1990).

[25]D.-S. Wang, R. Wu, and A. J. Freeman, Physical Review Letters **70**, 869 (1993).
[26]D.-s. Wang, R. Wu, and A. J. Freeman, Physical Review B **47**, 14932 (1993).
[27]P. Bruno, Physical Review B **39**, 865 (1989).
[28]T. Kosugi, T. Miyake, and S. Ishibashi, Journal of the Physical Society of Japan **83**, 044707 (2014).
[29]K. D. Belashchenko, L. Ke, M. Däne, L. X. Benedict, T. N. Lamichhane, V. Taufour, A. Jesche, S. L. Bud'ko, P. C. Canfield, and V. P. Antropov, Appl. Phys. Lett. **106**, 062408 (2015).
[30]O. K. Andersen, Phys. Rev. B **12**, 3060 (1975).
[31]I. Turek, V. Drchal, J. Kudrnovsky, M. Sob, and P. Weinberger, *Electronic Structure of Disordered Alloys, Surfaces and Interfaces* (Kluwer, Boston, 1997).
[32]D. Pashov, S. Acharya, W. R. L. Lambrecht, J. Jackson, K. D. Belashchenko, A. Chantis, F. Jamet, and M. van Schilfgaarde, Computer Physics Communications **249**, 107065 (2020).
[33]J. P. Perdew, K. Burke, and M. Ernzerhof, Phys. Rev. Lett. **77**, 3865 (1996).
[34]O. Jepson and O. K. Anderson, Solid State Commun. **9**, 1763 (1971).
[35]P. E. Blöchl, O. Jepsen, and O. K. Andersen, Phys. Rev. B **49**, 16223 (1994).